Soft-Switching and Efficient Power Transfer in Capacitive Wireless Systems with LCLC Compensation Networks

Eli Abramov, *Student Member*, *IEEE*,
Mor Mordechai Peretz, *Member*, *IEEE*

The Center for Power Electronics and Mixed-Signal IC,
Department of Electrical and Computer Engineering
Ben-Gurion University of the Negev
P.O. Box 653, Beer-Sheva 8410501, Israel
eliab@post.bgu.ac.il, morp@bgu.ac.il
http://www.ee.bgu.ac.il/~pemic

Ilya Zeltser, Member, *IEEE*

Power Electronics Department
Rafael Advanced Defense Systems Ltd.
P.O. Box 2250, Haifa 31021, Israel
ilyaz@rafael.co.il
www.rafael.co.il

***Abstract*—This study delineates the conditions for soft-switching in capacitively-coupled resonant converters that are compensated with *LCLC* matching networks. Such converters' setups are extremely popular in wireless capacitive power transfer (CPT) technology. The detailed analysis explores the intricate relationships between the parameters, operating conditions, and transfer characteristics. It reveals that by design of the compensation networks' parameters according to the highest expected coupling capacitance, then zero-voltage switching (ZVS) conditions are achieved over the entire operation range. The results of the analysis further outline the necessary conditions for zero-current switching (ZCS) at turn off. Consequently, the system maintains soft-switching both at turn on and turn off, for all switches. This provides a significant potential enhancement of the power transfer and processing efficiency, in particular for applications of wireless energy where the operating frequency is very high. The theoretical analysis and predictions have been verified by simulations and experimentally. The simulation platform incorporates a simple and flexible cross-coupled model, also developed in this study, which is used to evaluate the results under various conditions. The experiments have been carried out on a *LCLC* capacitive-based WPT prototype operated in the MHz range, and examined through several air-gaps up to 120 mm. An excellent agreement has been obtained between the theoretical work, simulations and the experimental evidence.**

Keywords — capacitive power transfer, capacitive coupling, soft-switching, zero-voltage switching, zero-current switching, capacitive coupler model, LCLC compensation.

I. Introduction

Over the last few years, capacitive power transfer (CPT) is a rapidly growing technology in the field of wireless power transfer (WPT) [1]-[6]. CPT is an attractive near-field power transfer method which overcomes undesired Eddy currents and other electromagnetic interferences (EMI) that are associated with other magnetic based WPT methods. In addition to improved efficiency characteristics, CPT systems offer design flexibility with potentially lower volume and reduced construction complexity [4]-[6]. This makes CPT technology an attractive candidate for various wireless power applications, such as biomedical implants, in-track-moving systems, various batteries charging and many more [7]-[12].

To achieve better power transfer characteristics, CPT-based wireless systems operate at high frequency (several MHz) and employ resonant conversion. This is essential to accommodate the relatively low effective capacitance value of the capacitive medium (few pF), enhance the transmission range, and achieve reasonable efficiency. A fundamental building block of the resonant converter is a compensation network. It typically comprises a second or higher order reactance that connects and performs impedance-matching between a sourcing circuit to a loading one. Depending on the configuration, these networks serve many design objectives, such as reducing circulating energy in the converter [13], lower voltage and current stresses of the switches [14]. In WPT systems, compensation networks also provide additional degrees of freedom to interact between the primary and secondary circuits and compensate for: resonant frequency, Volt-Ampere ratings, constant-voltage/current output (load-independent operation), output power and system efficiency [3], [15]-[17].

One of the popular, and at the same time complex, compensation network structures for CPT is the so-called double-sided *LCLC* compensation [3], [5], as shown in Fig. 1. There, each side of the converter incorporates a T-type network, consists of *LCL* branch [6]. Combined with the parallel capacitance of the medium (or additional parallel capacitance), it results in cascaded *LC* arrangement. Although the structure is quite complex and involves a significant number of passive components, in this configuration the output power is proportional to the coupling coefficient, which is also loosely-coupled from the components' values [5], [6]. This is a significant benefit compared to other network setups [1]-[3]. In addition, the voltage and current stresses on the components are lower than in other methods, in particular when increasing the distance between the transmitting and receiving sides [1]-[3], [5], [6].

Since high-frequency operation is strongly associated with considerable switching losses, a mechanism that assures soft-switching for wide operation range, covering all loading cases, is mandatory. This assertion is further challenging in the context of CPT systems, where the parameters dynamically vary due to changes in distance or misalignment between the transmitting and receiving sides. To alleviate the losses

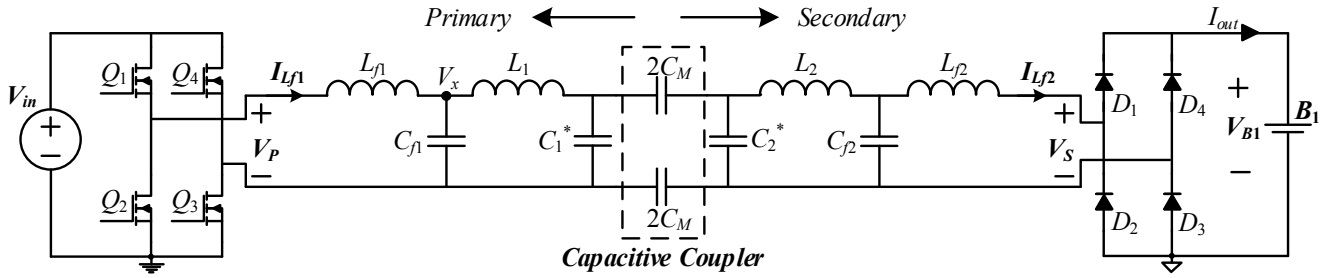

Fig. 1. Schematic diagram of a *LCLC* compensated capacitive WPT system.

associated with the commutation instances, it is required to consider the contributors of both turn on and turn off losses, and evaluate the conditions for both zero-voltage switching (ZVS) and zero-current switching (ZCS) under variations. Although several remedies of ZVS for CPT systems are discussed in the literature [3], [5], [6], a detailed analysis that covers the intricate relationships that impact soft-switching under variations and parameters sensitivity, has not been reported to-date. This has been pursued in this study.

The objective of this study is therefore to introduce comprehensive analysis on the conditions for soft-switching in *LCLC* compensated capacitive WPT system. The analysis methodology is to explore the affecting factors on the current at the turn off instance, and consequently, outline the requirements for soft-switching at turn on and turn off. This is achieved without compromising the overall performance of the system. It is a further objective of this study to present a simulation-compatible model of the capacitive coupler that enables visualization and evaluation of the system under (and through) variations of the parameters.

The rest of the paper is organized as follows: Following a brief survey of *LCLC* compensated CPT system, Section II details the analysis for the contributors of the soft-switching conditions. The description of the simulation model that has been developed for the *LCLC* WPT system is delineated in Section III. It is then followed by a simulation case study that highlights some of the system's interrelations. Experimental validation of the theoretical analysis and *LCLC* CPT prototype are provided in Section IV. Section V concludes the paper.

II. Soft-Switching Analysis

A resonant capacitive *LCLC* WPT system is shown in Fig. 1. The system is driven by a full-bridge inverter (Q_1-Q_4) on the primary side, and the load which in this case is considered as a battery, B_1, is fed through a diode rectifier (D_1-D_4) that is connected to the secondary's compensation network. Both the primary and secondary side are compensated by *LCLC* resonators (L_{f1}, C_{f1}; L_1, C_1^*; L_{f2}, C_{f2}; L_2, C_2^*). The capacitive coupler in this study is implemented by two pairs of plates [2], [6]. Assuming that the two pairs are placed sufficiently far from each other, the interconnection and fringe capacitances between the pairs can be neglected. Therefore, the capacitive coupler can be considered as two series capacitors as shown in Fig. 1, there, C_M is the mutual coupling capacitance.

The conditions for ZVS operation of the full-bridge switches is evaluated by the primary's side current, I_{Lf1}, at the commutation instance. That is, a necessary condition to achieve ZVS is that the current I_{Lf1} is positive while turning off the switches Q_1 and Q_3 (the negative transition of V_P), or that the current I_{Lf1} is negative while turning off the switches Q_2 and Q_4 (the positive transition of V_P). The current I_{Lf1} can be obtained from Fig. 1 as follows:

$$\frac{dI_{Lf1}(t)}{dt} = \frac{V_P(t) - V_x(t)}{Lf_1}. \tag{1}$$

In [6], it has been established that the capacitive coupler can be modeled as a two-port network as depicted in Fig. 2a. With the aid of this two-port representation, assuming high quality factor of the input and the output filters L_{f1}, C_{f1} and L_{f2}, C_{f2}, respectively, and by applying fundamental harmonics approximation (FHA) method [18], the system can be further simplified as shown in Fig. 2b. There, V_{P1} and V_{S1} represent the first harmonics sources of the square waves V_P and V_S (Fig. 1), whereas $V_P = 4V_{in}/\pi$ and $V_S = 4V_{B1}/\pi$. It should be noted that, in the equivalent circuit model the capacitances C_1 and C_2 are defined as $C_1^* + C_M$ and $C_2^* + C_M$, respectively.

Applying superposition theorem, the phasor representation of V_x can be expressed as:

$$\overrightarrow{V_x} = \frac{(Z_{L1} + Z_{C1}) \parallel Z_{Cf1}}{(Z_{L1} + Z_{C1}) \parallel Z_{Cf1} + Z_{Lf1}} \overrightarrow{V_{P1}} + \left(Z_{C1} \parallel (Z_{L1} + Z_{Lf1} \parallel Z_{Cf1})\right) \overrightarrow{I_1}, \tag{2}$$

where Z_{Cx} and Z_{Lx} are the impedances of the capacitors and inductors in Fig. 2b. Rearranging (2), V_x can be written as

$$\overrightarrow{V_x} = \frac{1 - \omega_r^2 L_1 C_1}{-\omega_r^2 L_{f1} C_1} \overrightarrow{V_{P1}} + \frac{C_M}{C_1} \overrightarrow{V_2}, \tag{3}$$

where ω_r is the angular operating frequency and V_2 is the voltage applied to the secondary's plates. Rewriting (3) for the absolute value of V_x yields

$$|V_x| = \sqrt{\left(\frac{1 - \omega_r^2 L_1 C_1}{-\omega_r^2 L_{f1} C_1} V_{in}\right)^2 + \left(\frac{C_M}{C_1} V_2\right)^2 + 2\frac{1 - \omega_r^2 L_1 C_1}{-\omega_r^2 L_{f1} C_1} \frac{C_M}{C_1} V_{in} V_2 \cos\theta}, \tag{4}$$

where Θ is the phase shift between V_{P1} and V_2. The phase shift, γ, between V_{P1} and V_x, is derived from (3) as follows

$$\gamma = \arcsin\left(\frac{C_M V_2}{C_1 V_x} \sin\theta\right). \tag{5}$$

From (3) and (5), the instantaneous voltage $V_x(t)$ can be expressed as

$$V_x(t) = |V_x| \sin(\omega t + \gamma). \tag{6}$$

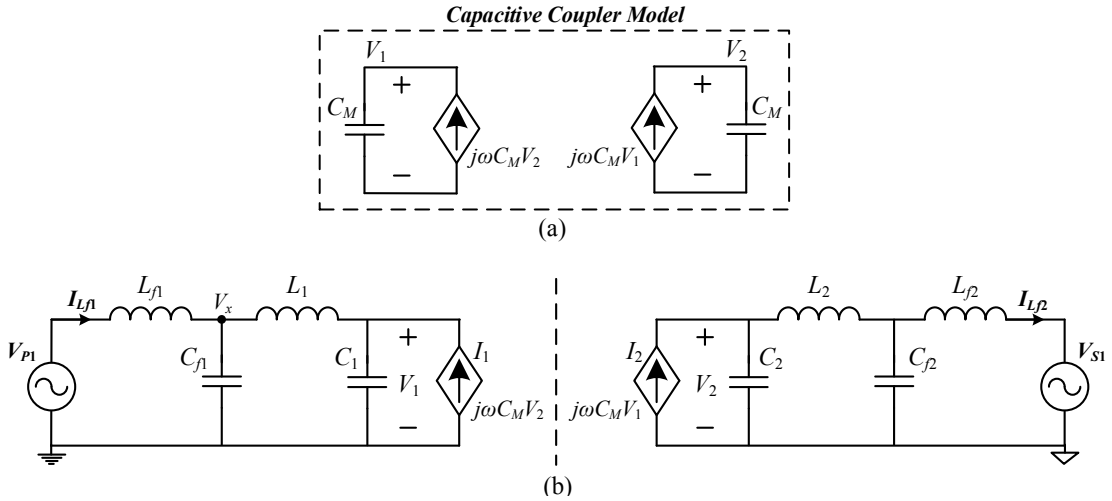

Fig. 2. (a) Two-port model of the capacitive coupler; (b) Simplified electrical model of a *LCLC* compensated CPT system by applying FHA analysis.

By substituting (6) into (1), the current I_{Lf1} can be expressed as follows

$$I_{Lf1}(t)=\frac{1}{L_{f1}}\left(V_{in}\cdot t+\frac{V_x}{\omega_r}\cos(\omega_r t+\gamma)-\frac{V_{in}\cdot\pi}{2\omega_r}\right). \qquad (7)$$

Finally, the current at the switching event, I_{sw}, is obtained from (7) by assuming $t = \pi/\omega$ (half a switching period). This yields

$$I_{sw}=\frac{1}{L_{f1}}\left(\frac{V_{in}\cdot\pi}{2\omega}-\frac{|V_x|}{\omega}\cos\gamma\right). \qquad (8)$$

Fig. 3 shows the switching current I_{sw} curve as a function of the capacitive coupling C_M, which has been plotted using (8). It follows from Fig. 3 that the switching current decreases as the coupling capacitance increases. This implies that once the CPT system is designed to operate at ZVS conditions for the maximum expected value of C_M (i.e. for the smallest air-gap), ZVS is guaranteed over the entire operating air-gaps.

Fig. 3 shows the switching current I_{sw} curve as a function of the capacitive coupling C_M, which has been plotted using (8). It follows from Fig. 3 that the switching current decreases as the coupling capacitance increases. This implies that once the CPT system is designed to operate at ZVS conditions for the maximum expected value of C_M (i.e. for the smallest air-gap), ZVS is guaranteed over the entire operating air-gaps.

It follows from the analysis in (4), (5) and (8), that I_{sw} can be adjusted by alternating the value of any reactive element at either the primary or the secondary sides of the CPT system. By doing so, I_{sw} can be kept at near zero-current value (enough to discharge the body capacitors of the switches), such that the switches are turned off at ZCS. That is, by applying this technique, the full-bridge can be operated at soft-switching at both turn on and turn off events, further reducing the switching losses. In this study, the value of the inductance L_1 is adjusted for different coupling capacitors C_M.

III. Simulation-Compatible Model of *LCLC* CPT System

To better view the implications of variations in the coupling capacitance and to observe sequential scenarios seamlessly, the

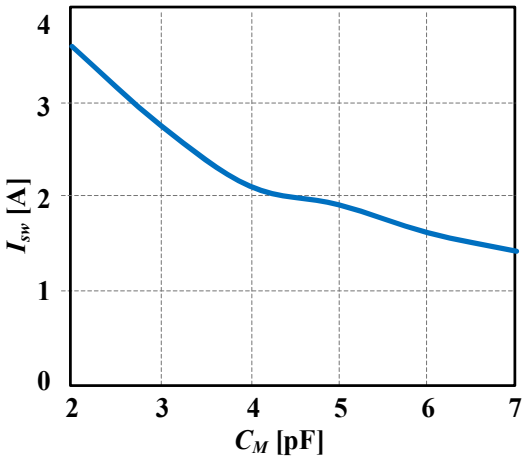

Fig. 3. The switching current I_{sw} as a function of the capacitive coupling (air-gap). List of the parameters used to obtain the curve are identical to the simulations and experiments and listed in Section III. □ is calculated from the simulation.

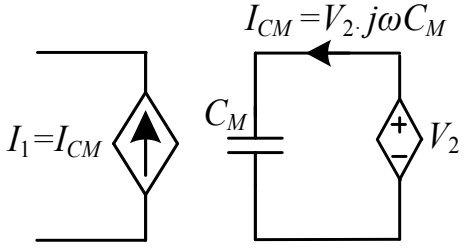

Fig. 4. Capacitive coupler equivalent simulation-compatible electrical model.

two-port network model of the capacitive coupler has been realized PSIM platform (PowerSim, Inc.). This also allows to perform a comprehensive analysis on the conditions for soft-switching. The capacitive voltage-dependent current source I_1 at the primary side of the coupler (Fig. 2) is generated as shown in Fig. 4 by replicating the current of an auxiliary capacitor, emulating the coupling capacitor C_M, which is exposed to the voltage V_2. In a similar manner, the capacitive voltage-dependent current source I_2 at the secondary side of the coupler (Fig. 2) is generated by exposing another auxiliary coupling capacitor C_M to the voltage V_1. This enables to evaluate the CPT

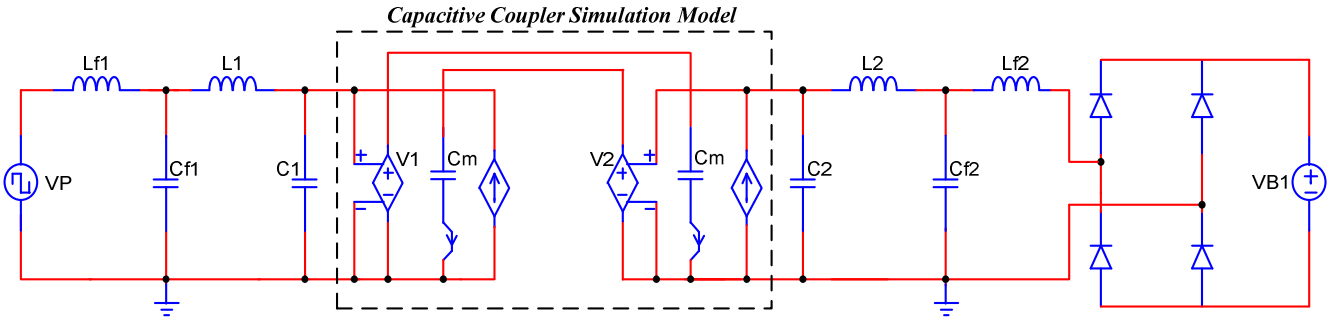

Fig. 5. Simulation-compatible model of the of the *LCLC* WPT system in PSIM platform.

system in time-domain simulation, under different operating conditions, with a coupler model that includes the amplitudes, but more importantly, the phase shifts on-the-fly.

Having a two-port capacitive coupler model, a cycle-by-cycle simulation test-bench for *LCLC* compensated capacitive WPT system has been constructed as shown in Fig. 5. It is assumed that coupling capacitance C_M is relatively small compared to the values of C_1^* and C_2^*. That is, $C_1^*= C_1$ and $C_2^*= C_1$ while varying the value of C_M for the various simulations. The system parameters of the simulation test-bench are as follows: both input and output battery are 50V, i.e., V_P toggles between -50 and 50 V, at operating frequency f_r =1.5 MHz. Based on the outlines that have been established earlier in analysis section II, to guarantee ZVS conditions over the entire coupling range then L_1 is set to be L_1=59.4 µH, the rest of the compensation networks values are $L_{f1}= L_{f2}$=1.25 µH, $C_{f1} =C_{f2}$=9 nF; L_2=60 µH, $C_1 =C_2$ =190 pF.

The first set of simulations has been carried out by varying the capacitive coupler. Fig. 6 shows the primary side simulation waveforms of voltage V_P and current I_{Lf1} for coupling capacitances of 2 pF and 7 pF. It can be seen that, for both cases ZVS is obtained. The conditions for 2 pF the current at turn off is 3.6 A, whereas it is 1.4 A for 7 pF.

The second set of measurements has been carried out by adjusting the inductor L_1 to obtain constant turn off current I_{sw} =1-A, over different values of C_M according to the soft-switching analysis presented in Section II. The results for these measurements are summarized in Table I. Fig. 7 depicts the simulation waveforms of voltage V_P and current I_{Lf1} for coupling capacitances of 2 pF and 7 pF. It can be seen that, for both C_M's ZVS as well as ZCS are now obtained, whereas target turn off current of 1-A as maintained constant. Very good agreement is demonstrated for various operating conditions between the theoretical soft-switching analysis and simulation outcomes.

TABLE I – ADJUSTED INDUCTOR L_1 VALUES TO OBTAIN ZCS AT CONSTANT CURRENT FOR VARIOUS C_M

C_M [pF]	2	3	4	5	6	7
L_1 [µH]	60	59.6	59.2	58.7	58.1	57.3
I_{sw} [A] Simulation	1	1	1	1	1	1
I_{out} [A]	0.275	0.75	1.15	1.42	1.508	1.64

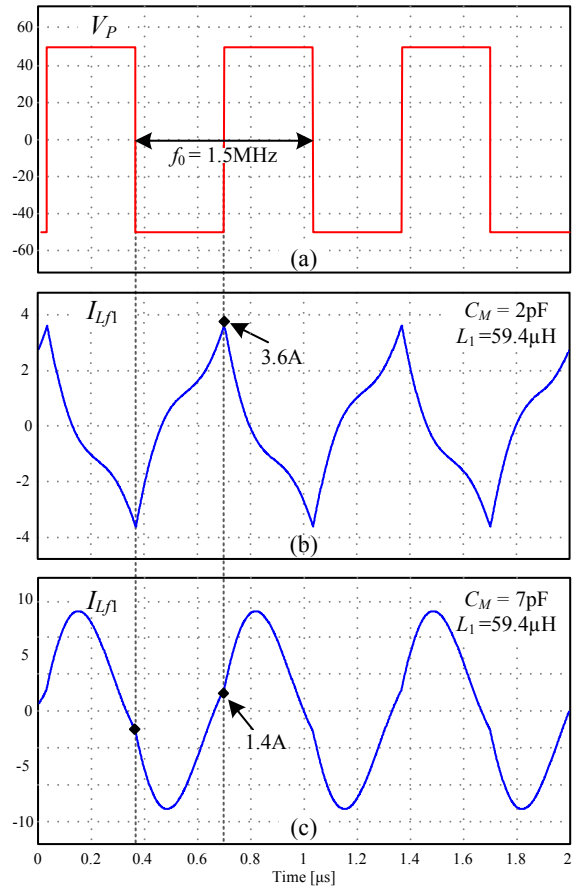

Fig. 6. Simulation waveforms of the primary side demonstrating ZVS for constant inductor L_1=59.4 µH: (a) voltage V_P, (b) current I_{Lf1} for C_M=2 pF, (c) current I_{Lf1} for C_M=7 pF.

IV. EXPERIMENTAL VERIFICATION

An experimental *LCLC* capacitive WPT prototype has been constructed (Fig. 8) to further validate and examine the derived criteria to facilitate soft-switching. Four symmetrical copper plates form the capacitive coupling, whereas each plate is 25x25 cm. The compensation networks have been designed according to the case study in Section III. The gate drive control signals of the full-bridge inverter were generated using Altera Cyclone IV FPGA [19], at an operating frequency f_r =1.5 MHz. It should be noted that to overcome magnetics limitations when operating in the MHz range [20], [21], all the inductors within the prototype have been constructed with a litz wire wrapped on an air-core. High-voltage multilayer SMD ceramic capacitors have been used for the compensation capacitors. The

...

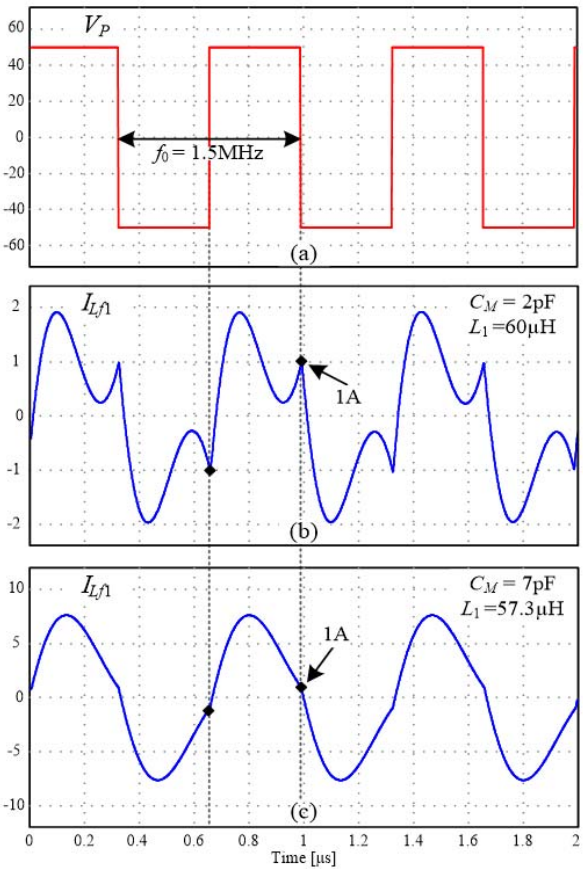

Fig. 7. Simulation waveforms of the primary side for tuned inductor L_1: (a) voltage V_P, (b) current I_{Lf1} for C_M=2 pF and L_1=60 µH, (c) current I_{Lf1} for C_M=7 pF and L_1=57.3 µH.

overall experimental prototype parameters are summarized in Table II.

Typically in such CPT systems high-Q operation as well as high-electric fields are naturally facilitated, thus, due to safety issues, the first set of experiments has been carried out for lower input voltage settings V_{in}=10-V. Fig. 9 depicts the values of the current I_{Lf1} at a turn off switching event (I_{sw}) for different values of the mutual coupling capacitance C_M, which approximately translates to air-gaps of 30 mm up to 100 mm, while L_1=60 µH. It can be well observed that for higher values of C_M, the switching current decreases and soft-switching conditions are not obtained, well validating the theoretical analysis.

Next, in the second experiment, the inductor L_1 has been adjusted to satisfy ZVS conditions over the entire coupling range, that is, adjusting L_1 according to the highest C_M (7 pF). Fig. 10 shows experimental waveforms of the primary side voltage V_P and current I_{Lf1} for two different coupling capacitances (2 pF and 7 pF). As can be observed, for both cases ZVS is obtained. The conditions for 2 pF the current at turn off is 1.3-A, whereas it is 0.22-A for 7 pF.

To further validate the soft-switching analysis, by adjusting the inductor L_1 using the relationships given in (5), (6) and (8), the current at turn off has been calibrated to be constant in the vicinity of 0.2-A, guaranteeing virtually ZCS over the coupling operating range. The resulting inductor L_1 values for the entire given C_M range are as summarized in Table I, whereas the difference is in the current levels due to the different input voltage. Fig. 11 depicts experimental waveforms of the primary

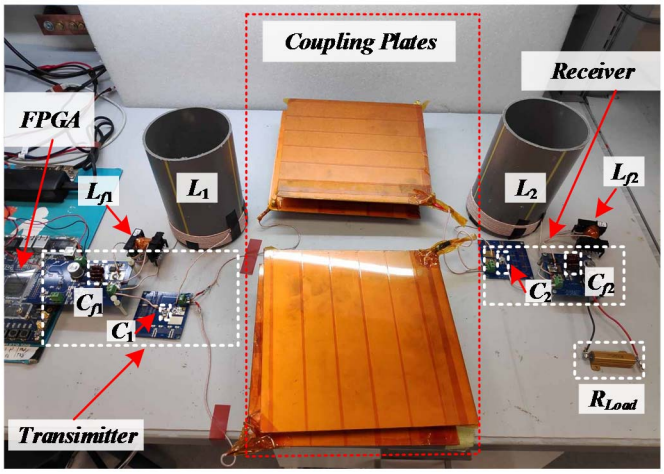

Fig. 8. Experimental setup of a *LCLC* compensated capacitive WPT prototype.

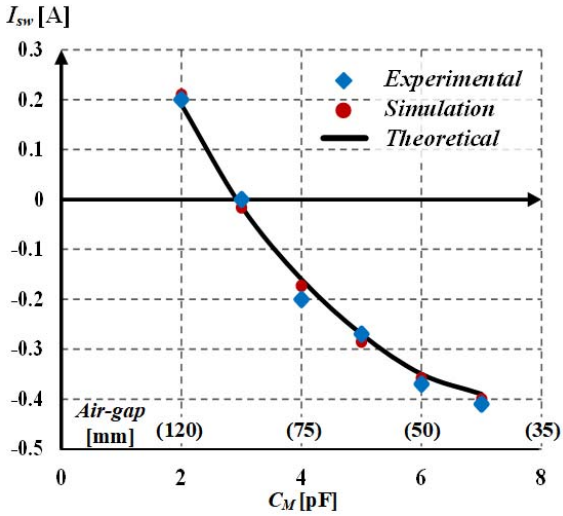

Fig. 9. Measured current I_{sw} for L_1 =60µH and various mutual coupling capacitance C_M.

for C_M=2 pF and L_1=60 µH, as can be observed soft-switching is satisfied while both ZVS and ZCS are obtained such that the current at turn off I_{sw}≈ 0.2-A. The experimental results tightly follow the results obtained by the simulations as well as the theoretical predictions.

TABLE II – EXPERIMENTAL PROTOTYPE SPECIFICATIONS AND PARAMETERS

Parameter	*Design Value*
Input voltage V_{in}	10-V
Coupling plates	25x25 cm
Full-bridge transistors	LMG5200, 80-V
Operating frequency f_r	1.5 MHz
Lf_1 , Lf_2	1.25 µH
L_1 , L_2	57.3-60 µH, 60 µH
Cf_1 , Cf_2	9 nF
C_1 , C_2	190 pF

V. CONCLUSION

Comprehensive soft-switching analysis of a resonant converter with a double-sided *LCLC* compensation network, which has been employed for capacitively-coupled wireless power transfer has been presented. A detailed criteria for soft-

...

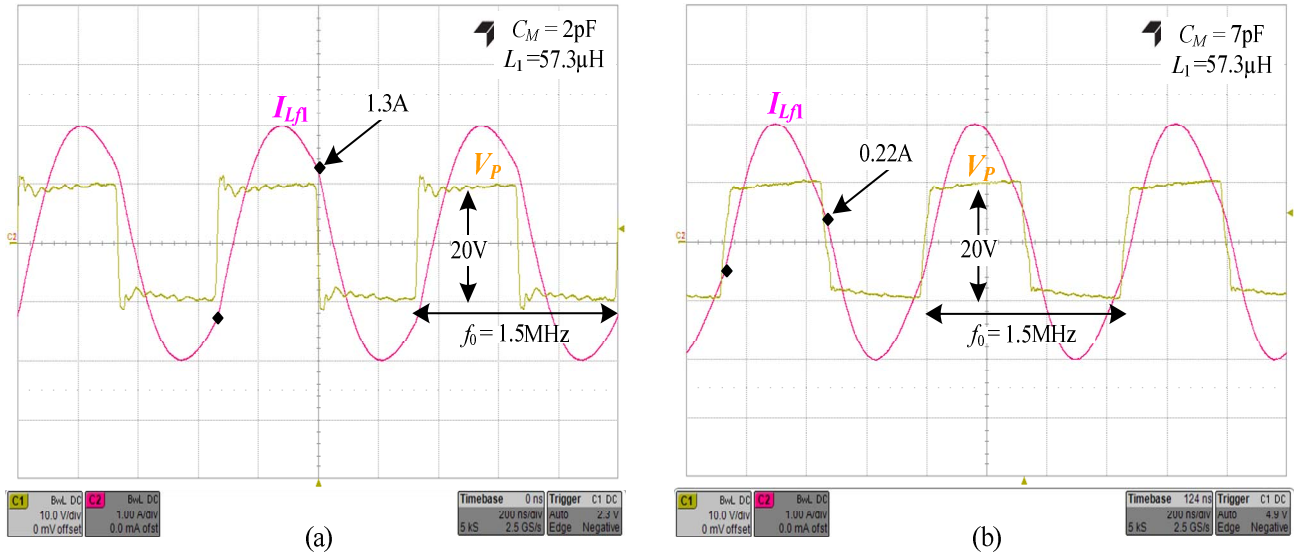

Fig. 10. Experimental waveforms of the primary side voltage V_P (yellow curve – 10V/div) and current I_{Lf1} (pink curve – 1A/div) for L_1 =57.3 µH: (a) C_M=2pF, (b) C_M= 7pF and. Time scale 200ns/div.

switching has established that, ZVS is achieved over the entire operating range if the system's parameters are designed for the highest expected coupling capacitor. It follows from the analysis presented in this study, that the current at turn off can be kept low for various operating conditions assisting ZCS at turn off. This way, soft-switching is obtained at both turn on and turn off of the full-bridge switches, further reducing the switching losses. The analysis has been validated by simulation as well as by various experiments up to 120mm air-gap. Very good agreement is found between the theoretical predictions and the experimental and simulation results.

ACKNOWLEDGEMENT

This research was supported by The Prof. A. Pazi Research Foundation.

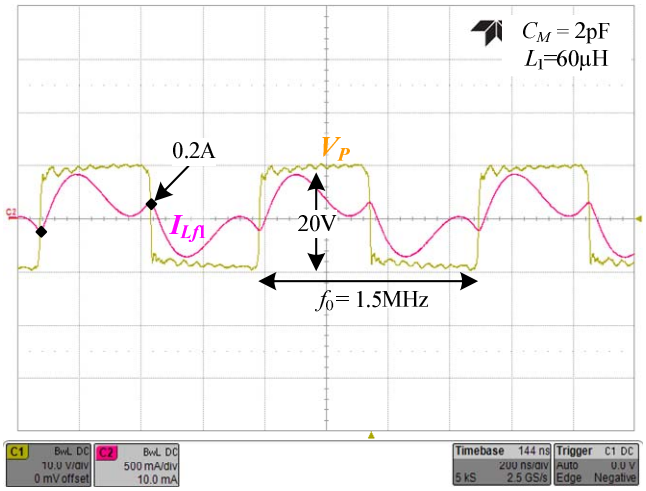

Fig. 11. Experimental waveforms of the primary side voltage V_P (yellow curve – 10V/div) and current I_{Lf1} (pink curve – current scale 0.5A/div) for C_M=2 pF and L_1=60 µH. Time scale 200ns/div.

REFERENCES

[1] F. Lu, H. Zhang, H. Hofmann, C. Mi, "A loosely coupled capacitive power transfer system with LC compensation circuit topology," *Proc. IEEE Energy Convers. Congr. Expo. (ECCE)*, pp. 1-5, 2016.

[2] F. Lu, H. Zhang, C. Mi, "A two-plate capacitive wireless power transfer system for electric vehicle charging Applications," *IEEE Trans. Power Electron*, vol. 33, no. 2, pp. 946-969, Aug. 2017.

[3] F. Lu, H. Zhang, H. Hofmann, and C. Mi, "A double-sided LC compensation circuit for loosely-coupled capacitive power transfer," *IEEE Trans. Power Electron*., vol. 33, no. 2, pp. 1633 – 1643, Feb. 2017.

[4] M. P. Theodoridis, "Effective capacitive power transfer," *IEEE Trans. Power Electron*., vol. 27, no. 12, pp. 4906–4913, Dec. 2012.

[5] F. Lu, H. Zhang, H. Hofmann, and C. Mi, "A double-sided *LCLC* compensated capacitive power transfer system for electric vehicle charging," *IEEE Trans. Power Electron.*, vol. 30, no. 11, pp. 6011–6014, Jun. 2015.

[6] H. Zhang, F. Lu, H. Hofmann, W. Liu, and C. C. Mi, "A four-plate compact capacitive coupler design and LCL-compensated topology for capacitive power transfer in electric vehicle charging application," *IEEE Trans. Power Electron*., vol. 31, no. 12, pp. 8541–8551, Dec. 2016.

[7] A. M. Sodagar and P. Amiri, "Capacitive coupling for power and data telemetry to implantable biomedical microsystems," in *Proc. 4th Int. IEEE/EMBS Conf. Neural Eng.*, Apr. 29–May 2, 2009, pp. 411–414.

[8] Liu. Chao, A. P. Hu, and M. Budhia, "A generalized coupling model for capacitive power transfer systems," in *Proc. 36th Annu. Conf. IEEE Ind. Electron. Soc*., Nov.7–10, 2010, pp. 274–279.

[9] S. Li and C. Mi, "Wireless Power Transfer for Electric Vehicle Applications," *IEEE Journal of Emerging and Selected Topics in Power Electronics*, vol. PP, pp. 1-1, 2014.

[10] S. Jaegue et al., "Design and implementation of shaped magnetic resonance-based wireless power transfer system for roadway-powered moving electric vehicles," *IEEE Trans. Ind. Electron*., vol. 61, no. 3, pp. 1179–1192, Mar. 2014.

[11] S.Y.R. Hui, W. Zhong and C.K. Lee, "A critical review of recent progress in mid-range wireless power transfer," *IEEE Transactions on Power Electronics*, vol. 29, no. 9, pp. 4500-4511, September 2014.

[12] F. Musavi and W. Eberle, "Overview of wireless power transfer technologies for electric vehicle battery charging," *IET Power Electronics*, vol. 7, no. 1, pp. 60–66, 2014.

• • •

[13] C. Lin and F. Lee, "Design of a piezoelectric transformer converter and its matching networks," *Proc. IEEE-PESC'94 Conf.*, vol. 1, pp. 607–612, 1994.
[14] M. Evzelman and M. M Peretz "Optimal design of a class-E resonant driver," *IET Power Electronics,* vol. 8, no.8, pp 1552-1557, Apr. 2015.
[15] W. Zhang and C. Mi, "Compensation topologies for high power wireless power transfer systems," *IEEE Transactions on Vehicular Technology*, vol. 65, no.6, pp. 4768-4778, July 2015.
[16] S. Sinha, A. Kumar, S. Pervaiz, B. Regensburger and K.K. Afridi, "Design of efficient matching networks for capacitive wireless power transfer systems," *Proceedings of the IEEE Workshop on Control and Modeling for Power Electronics (COMPEL)*, Trondheim, Norway, June 2016.
[17] A. Kumar, S. Sinha, A. Sepahvand, K. K. Afridi, "Improved design optimization for high-efficiency matching networks," *IEEE Transactions on Power Electronics*, vol. 33, no. 1, pp. 37-50, Jan 2018.
[18] R. L. Steigerwald, "A comparison of half-bridge resonant converter topologies," *IEEE Transactions on Power Electronics*, vol. 3, no. 2, pp. 174-182, April 1988.
[19] DE2 development and education board user manual, Altera Corporation, 2006.
[20] J. Craninckx and M. Steyaert, "A 1.8-GHz low-phase-noise CMOS VCO using optimized hollow spiral inductors," *IEEE J. Solid-State Circuits,* vol. 32, pp. 736–744, May 1997.
[21] M. Bartoli, N. Noferi, A. Reatti, and M. Kazimierczuk, "Modeling litzwire winding losses in high-frequency power inductors," in *Proc. IEEE Power Electronics Specialists Conf.*, Jun. 23–27, 1996, pp. 1690–1696.